Oxidative Folding Pathway of Onconase, a Ribonuclease Homologue: Insight into Oxidative Folding Mechanisms from a Study of Two Homologues[†]

Robert F. Gahl and Harold A. Scheraga*

Baker Laboratory of Chemistry, Cornell University, Ithaca, New York 14853

Received December 20, 2008; Revised Manuscript Received February 18, 2009

ABSTRACT: The oxidative folding pathways of two four-disulfide proteins of the ribonuclease family, ONC and RNase A, which have similar three-dimensional folds but only 30% sequence homology, are compared. In this study, a mechanism for the oxidative folding pathway of ONC is proposed. In particular, the kinetic roles and thermodynamic characteristics of key intermediates along the oxidative folding pathway, specifically, the structured intermediates, I_1, I_2, and I_3, previously identified as des-[19−68,30−75], des-[30−75], and des-[19−68], respectively, are discussed. In addition, the effects of temperature on the oxidative folding pathway have been examined. Differences in the folding mechanism between ONC and RNase A are attributed to the differences in their amino acid sequences and related inter-residue interactions, including differences in hydrophobic interactions. Compared to RNase A, ONC utilizes more efficient interactions along the oxidative folding pathway to adopt its native fold more rapidly.

By examining the oxidative folding pathways of two homologues of the ribonuclease family, ONC[1] in this paper, compared with our earlier work on RNase A (*1, 2*), we gain insight into oxidative folding of proteins. Of special interest in comparing these two four-disulfide proteins with the same tertiary fold (Figure 1), but with only 30% sequence homology (*3*), is the fact that three of the four native disulfide bonds ([19−68], [30−75], and [48−90] of ONC and [26−84], [40−95], and [58−110] of RNase A) are in structurally homologous positions. The fourth native disulfide bond ([65−72] of RNase A), which closes a loop in the interior of the backbone, is replaced by the [87−104] disulfide bond of ONC, which closes the C-terminal region of the protein (see Figure 1). Further, since the [65−72] disulfide bond of RNase A is the first one to form in the oxidative folding pathway (*4*), ONC must fold by another oxidative pathway because it lacks this homologous disulfide bond. Clearly, the differences in the amino acid sequences of these two structurally homologous proteins must account for anticipated differences in their oxidative folding pathways. Therefore, the goal of this investigation was to characterize the oxidative folding pathway of ONC, by identifying the kinetic mechanism by which ONC attains the correct disulfide bonding, coupled with the attainment of the nativelike structure, thereby providing an understanding of the physicochemical properties of two members of the ribonuclease family.

An additional interest in ONC is the discovery that ONC is cytotoxic to various cancerous cell lines under in vivo conditions (*3*). As a result, ONC has undergone clinical trials for the treatment of unresectable malignant mesothelioma (UMM). The clinical trials have just been completed, and a new drug application is being submitted (*5*). Current research has focused on understanding the critical steps in the cytotoxic action of ONC on cancerous cells (*6, 7*). The efficacy of the cytotoxicity of ONC is due to its selective uptake into cancerous cells and its resistance to proteolysis in regulatory pathways after undergoing endocytosis (*3*). One drawback to ONC is that it is not as effective as a catalyst compared to the catalytic activity of other ribonucleases such as RNase A. Efforts have been made to increase the catalytic efficiency of ONC. However, the catalytic efficiency of RNase A has not been matched (*8, 9*). Further work to understand the physicochemical properties of members of the ribonuclease family would aid continuing work to utilize ribonucleases as chemotherapeutics.

In our laboratory, RNase A has been used as a model system to study the protein folding problem. In particular, RNase A has been used to develop methods for studying the oxidative folding of disulfide-bond-containing proteins to determine how they attain both the correct disulfide linkages and the biologically active structure from a reduced form having no disulfide bonds. By application of these methods to RNase A, two types of intermediate species along the oxidative folding pathway have been identified and characterized: unstructured ensembles (*n*S) and structured

[†] This work was supported by NIH Grant GM-24893.

* To whom correspondence should be addressed. Telephone: (607) 255-4034. Fax: (607) 254-4700. E-mail: has5@cornell.edu.

[1] Abbreviations: ONC, frog onconase (*Rana pipiens*); R-ONC, onconase with all its disulfide bonds reduced; RNase A, bovine pancreatic ribonuclease A; AEMTS, 2-aminoethylmethylthiosulfonate; DTT^{ox} and DTT^{red}, oxidized and reduced dithiothreitol, respectively; GdnHCl, guanidine hydrochloride; Tris, tris(hydroxymethyl)aminomethane; HEPES, *N*-(2-hydroxyethyl)piperazine-*N*′-(2-ethanesulfonic acid); DTNB, 5,5′-dithiobis(2-nitrobenzoic acid); TNB, 2-nitro-5-mercaptobenzoic acid; NTSB, disodium 2-nitro-5-thiosulfobenzoate; MRE, mean residue ellipticity; TFA, trifluoroacetic acid; SCX, strong cation exchange; RP, reversed phase; HPLC, high-performance liquid chromatography; des-[*a*−*b*,*c*−*d*], species that contains all native disulfide bonds except for the *a*−*b* and *c*−*d* disulfide bonds; *n*S, unstructured ensemble of disulfide-containing intermediates each having *n* disulfide bonds; *n*S*, single structurally folded intermediate species containing *n* native disulfide bonds; N, native onconase; PDB, Protein Data Bank.

10.1021/bi802327j CCC: $40.75
Published on Web 03/10/2009

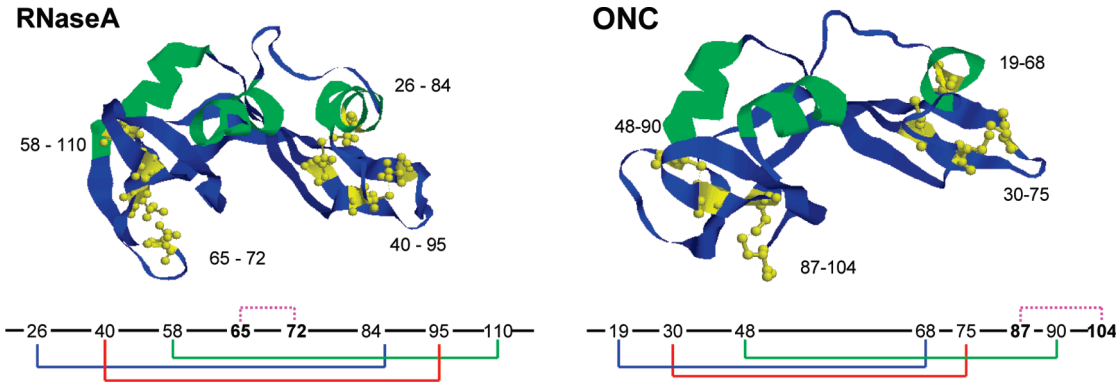

FIGURE 1: Crystral structures of RNase A, 124 residues (PDB entry RSA1), and ONC, 104 residues (PDB entry 1ONC). Disulfide bonds are shown as ball-and-stick models. The disulfide bond connectivity is shown below the corresponding crystal structure.

species (*n*S*). The oxidative folding mechanism of RNase A has been established in terms of these types of species (*1, 2, 10, 11*). In the early stages of oxidative folding, a pre-equilibrium between unstructured ensembles with zero, one, two, three, and four disulfide bonds is established. Each of these ensembles, except the fully reduced form, contains native and non-native disulfide bonds. The rate-determining step in the mechanism was identified (*1*) as a redox-independent SH/S−S reshuffling step from an unstructured ensemble (3S) to two structured species (*2*), des-[40−95] and des-[65−72], each designated as 3S*, which oxidize rapidly to the native form. The structured 3S* intermediates have been analyzed by NMR (*12, 13*). Further work is being carried out to identify the residues responsible for the stabilization of these structured species (R. F. Gahl, R. E. Oswald, and H. A. Scheraga, work in progress).

Methods developed for the study of the oxidative-folding process in RNase A have been applied for the separation and purification of key disulfide bond species in the oxidative folding of ONC. In a previous study (*14*), three structured intermediate species, des-[19−68, 30−75], des-[30−75], and des-[19−68], of ONC were identified. In this study, their thermodynamic stabilities are characterized with the use of CD spectroscopy, and their roles in the kinetic pathways are identified. In addition, the temperature dependence of the folding mechanism is also studied. By analyzing the effect of temperature on the various folding stages, we identify the nature of the interactions in key species that drive the folding. The information gained from these studies improves our understanding of the physicochemical properties of the ribonuclease fold.

MATERIALS AND METHODS

Materials. Wild type onconase was prepared from cDNA kindly provided by R. J. Youle (*15*) and purified as described previously (*14, 16*). DTT^{ox} was purified by RP-HPLC to 99.999% as confirmed by RP-HPLC and Ellman analysis (*17*). All other highest-quality chemicals were purchased from Sigma, Fisher, and Anatrace and used without any further purification.

Preparation of Reduced Onconase. Reduced onconase, R-ONC, was prepared by adding lyophilized ONC to 4 mL of a buffer [0.1 M Tris and 1 mM EDTA (pH 8)] containing 6 M GdnHCl and 100 mM DTT^{red} (to an ONC concentration of 2 mg/mL) under humidified argon. After 2−4 h, the reduction was stopped by reducing the pH to 3 using 100 μL of glacial acetic acid and immediately desalting the mixture on a G25 size-exclusion column equilibrated with 50 mM acetic acid (pH 3) to avoid air oxidation. As soon as R-ONC eluted, it was frozen and stored at −70 °C. After the mixture had been desalted, water and acetic acid were removed by lyophilization, and R-ONC was stored as aliquots in 3 mM acetic acid at a concentration of 2.8 mg/mL at −70 °C. These aliquots were diluted to 17 μM (0.20 mg/mL) for oxidative folding experiments.

Two methods were used to measure the concentration of R-ONC: UV absorption at 280 nm and thiol content with Ellman's reagent (*17*). To determine the concentration of R-ONC by UV absorption, 7400 ± 600 M^{-1} cm^{-1} was used as the molar absorptivity, ε_{280}, at 280 nm, determined by fitting the linear region of an absorbance at 280 nm versus concentration curve to the Beer−Lambert equation. To determine the concentration of R-ONC by Ellman's analysis, a 15 μL aliquot of R-ONC stored in 3 mM acetic acid was added to 435 μL of a buffer [0.1 M Tris (pH 8.3)] that was previously purged of oxygen with humidified argon. A 50 μL aliquot of a 15 mM DTNB solution in 0.1 M Tris buffer (pH 8.3) was added to the 450 μL solution containing R-ONC. The thiol content of R-ONC was measured from the absorbance of TNB at 412 nm, using 13600 M^{-1} cm^{-1} (*17*) to determine the concentration of free TNB in the solution, which corresponds to the thiol content. The TNB concentration was divided by 8 (R-ONC has eight cysteines) to obtain the concentration of R-ONC. Each method gave the same concentration of R-ONC within experimental error (~5%).

Preparation of Solutions for Oxidative Folding. The oxidative folding of ONC was studied under an anaerobic environment in which the redox potential of the solution was controlled by the relative concentrations of DTT^{ox} and DTT^{red}. Tests were performed to verify (i) that there were only trace amounts of dissolved oxygen that would not affect the rate of oxidative folding over the course of the experiment and (ii) that the method used to purge oxygen from the solution did not affect the concentration of the oxidizing agents or of R-ONC during the oxidative folding process. Oxidative folding solutions, including DTT^{ox}, were purged with humidified argon before R-ONC, or in some cases DTT^{red} to control the redox conditions, was added to start the folding process. Also, as a control, DTT^{red} was added to a purged protein-free solution to make sure that oxygen had been removed by the purging process. Under all of the

conditions used to study the oxidative folding of ONC, the extent of DTT^{red} oxidation by oxygen was no more than 5% for the duration of the oxidative folding experiments.

The mechanism for thiolate oxidation by DTT^{ox} is outlined in ref *10*. For every two thiolates that are oxidized by one molecule of DTT^{ox}, one molecule of DTT^{red} is produced. DTT^{red} can also react with disulfide bonds, and this is taken into account in analyzing the kinetics, mentioned later. Therefore, it is important to make sure that no dissolved oxygen reacts with the thiolate ions of oxidative folding intermediates or with the DTT^{red} that is produced, i.e., that the thiolate content remains constant throughout the duration of the oxidative folding experiment.

Oxidative folding was also studied over a range of temperatures. To ensure that the concentration of species in the folding solutions did not change with temperature, the concentration of a solution containing 5 mM DTT^{ox} [0.1 M Tris (pH 8.0)] was monitored over time at each temperature at 330 nm using a value of 22.3 M^{-1} cm^{-1} for the molar absorptivity of DTT^{ox}, determined by plotting the absorbance at 330 nm versus concentration according to the Beer−Lambert equation. In addition, the humidified argon had to be equilibrated at the temperature of the reaction before it was used to purge the solution of oxygen. The concentration of DTT^{ox} did not change by more than 5% over the duration of time used to monitor oxidative folding.

The pH of Tris buffer is temperature-dependent (*18*). For studies at different temperatures, this effect had to be taken into account to eliminate pH-dependent effects on the oxidative folding pathway. Our oxidation studies were performed at pH 8.0, which had to be kept constant at the different temperatures used. The temperature dependence of the pH of the buffer was measured at temperatures ranging from 15 to 57 °C. The slope ($\Delta pH/\Delta T$) of the pH versus temperature curve was determined to be -0.026 ± 0.0012 and is comparable to other values in the literature, −0.028 (*18, 19*). To adjust for this effect at different temperatures, the pHs of buffers containing 0.1 M Tris were adjusted to compensate for this variation from ambient temperature, 22 °C, to a given temperature to perform oxidative folding, at pH 8.0 at 15−57 °C; e.g., the pH of a buffer for a 15 or 37 °C experiment was adjusted to 7.7 or 8.3, respectively, at 25 °C.

Oxidative Folding of ONC and SCX−HPLC Analysis. The range of redox conditions used to elucidate the oxidative folding pathway of ONC, starting with R-ONC, was from 25 to 115 mM DTT^{ox} and from 0 to 66 μM DTT^{red} in the presence of 25 mM DTT^{ox}, at 25 °C. For studies at temperatures varying from 15 to 57 °C, the redox condition used was 25 mM DTT^{ox} and 16 μM DTT^{red}. The concentration of R-ONC was 17 μM in all experiments. Precipitation was observed in experiments at concentrations higher than 17 μM (unpublished results). To ensure that no precipitation occurred during the folding experiments, a UV−vis spectrum was taken at the beginning and end of the experiments. There was no change between each of the spectra. In addition, a constant thiolate content for the duration of the oxidative folding experiment was verified by measuring the thiolate content using Ellman's reagent at different times during the folding process.

After a redox solution was purged of oxygen by humidified argon, R-ONC, or in some cases DTT^{red}, was added to the folding mixture under a certain redox condition and folding was allowed to proceed. The reaction mixture was kept under humidified argon for the duration of the folding reaction. At certain times, an aliquot was removed and added to a blocking buffer [2 M Tris (pH 8.6) and 20 mM EDTA], which contained enough AEMTS to constitute a 100-fold molar excess with respect to the free thiol content in the mixture. The blocking buffer that contained the AEMTS was diluted 10-fold upon addition of an aliquot of the oxidative folding mixture. The blocking of the free thiols by AEMTS was allowed to proceed for 2 min. The blocking reaction was stopped by the addition of glacial acetic acid. The aliquots were then frozen and maintained at −70 °C and could be stored at this temperature. Before the aliquots could be analyzed, the frozen solution was thawed and the buffer salts and unreacted AEMTS were removed by desalting on a G25 size-exclusion column equilibrated with 0.2% acetic acid using absorbance at 280 nm to monitor the eluted species.

Complete blocking was verified by a negative Ellman's test. There was no absorbance at 412 nm, indicating that all of the free thiolates had been blocked by AEMTS. The effectiveness of desalting with a G25 column was verified by comparing an AEMTS-blocked aliquot desalted with the G25 column and an aliquot desalted by RP-HPLC, the latter being a more effective but more time-consuming procedure with which to desalt samples. Desalting by RP-HPLC was performed on a water/acetonitrile buffer system with 0.09% TFA using a 25 cm × 4.6 mm SULPELCO Discovery BIO Wide Pore C18, 5 mm particle size column and absorbance at 210 nm to monitor the eluting species, i.e., to demonstrate that salt had been removed. After the sample was injected with 100% water and 0% acetonitrile running through the column and the buffer salts, DTT^{ox}, AEMTS-blocked DTT^{red}, and unreacted AEMTS eluted off the column, a constant flow of 20% water and 80% acetonitrile was passed through the column to elute and collect the intermediate disulfide-bonded species of ONC. The acetonitrile, water, and TFA were removed by lyophilization before the protein species were reconstituted in 3 mM acetic acid to be analyzed by SCX−HPLC. Independent chromatograms of each of these protein-containing aliquots from both methods, analyzed by SCX−HPLC, were identical. Use of size-exclusion G25 columns was sufficient to analyze aliquots taken at different times during oxidative folding experiments.

After an aliquot from an oxidative folding mixture was blocked with AEMTS and properly desalted using a size-exclusion G25 column, it was loaded directly onto an SCX−HPLC system for separation and analysis using a TOSOH Biosciences TSKgelTM (SP-5PW 7.5 cm × 7.5 mm), analytical strong-cation-exchange (SCX) column. The running buffer consisted of 25 mM HEPES and 2 mM EDTA (pH 8). The gradient used to separate the various AEMTS-blocked species was 0 to 480 mM NaCl in 120 min. The running buffer of the size-exclusion G25 column, 3 mM acetic acid, is compatible with the SCX−HPLC column and buffer system. The amount of each species was estimated quantitatively by monitoring the absorbance at 280 nm, and the relative amounts of each species were computed by integrating the area of each corresponding peak. The observed intermediate species along the folding pathway

under conditions reported in the figure legend are indicated in Figure 2.

For one experiment, it was necessary to determine the products of the direct oxidation of unblocked I_1, i.e., des-[19−68,30−75], to N. To prepare a sufficient amount of unblocked I_1 from R-ONC, the oxidation of R-ONC was carried out with 25 mM DTT^{ox}, at 25 °C and pH 8.0, for 15 min. The subsequent oxidation of R-ONC was stopped by the addition of acetic acid. The products were separated by RP-HPLC as described above, the difference being that a gradient from 30 to 45% acetonitrile over 60 min, instead of a constant mixture of 20% water and 80% acetonitrile, was used to separate the unblocked species in the reaction mixture.

After unblocked I_1 was collected, water, TFA, and acetonitrile were removed by lyophilization. Unblocked I_1 was reconstituted in 50 mM acetic acid buffer, and its concentration (10 μM) was determined by Ellman's reagent. Using the procedure described above, the oxidation of I_1 to N was then examined.

Analysis of the Kinetics of Oxidative Folding. To determine the mechanism of oxidative folding of ONC, the observed redox-independent rate constants for the various steps in a kinetic scheme were determined under the redox conditions mentioned in the previous section. Via examination of various possible mechanisms, the following one was found to provide the best fit to the experimental variation of the concentrations of each species with time:

$$R + DTT^{ox} \underset{k_2}{\overset{k_1}{\rightleftharpoons}} 1S + DTT^{red} \quad (1)$$

$$1S + DTT^{ox} \underset{k_4}{\overset{k_3}{\rightleftharpoons}} 2S + DTT^{red} \quad (2)$$

$$1S + DTT^{ox} \underset{k_6}{\overset{k_5}{\rightleftharpoons}} I_1 + DTT^{red} \quad (3)$$

$$2S + DTT^{ox} \xrightarrow{k_7} I_3 + DTT^{red} \quad (4)$$

$$I_1 + DTT^{ox} \xrightarrow{k_8} I_2 + DTT^{red} \quad (5)$$

$$I_1 + DTT^{ox} \xrightarrow{k_9} I_3 + DTT^{red} \quad (6)$$

$$I_2 + DTT^{ox} \xrightarrow{k_{10}} N + DTT^{red} \quad (7)$$

$$I_3 + DTT^{ox} \xrightarrow{k_{11}} N + DTT^{red} \quad (8)$$

This mechanism can be described by the following system of differential equations:

$$\frac{dR}{dt} = -k_1[DTT^{ox}][R] + k_2[DTT^{red}][1S] \quad (9)$$

$$\frac{d1S}{dt} = k_1[DTT^{ox}][R] - k_2[DTT^{red}][1S] - k_3[DTT^{ox}][1S] + k_4[DTT^{red}][2S] - k_5[DTT^{ox}][1S] + k_6[DTT^{red}][I_1] \quad (10)$$

$$\frac{d2S}{dt} = k_3[DTT^{ox}][1S] - k_4[DTT^{red}][2S] - k_7[DTT^{ox}][2S] \quad (11)$$

$$\frac{dI_1}{dt} = k_5[DTT^{ox}][1S] - k_6[DTT^{red}][I_1] - k_8[DTT^{ox}][I_1] - k_9[DTT^{ox}][I_1] \quad (12)$$

$$\frac{dI_2}{dt} = k_8[DTT^{ox}][I_1] - k_{10}[DTT^{ox}][I_2] \quad (13)$$

$$\frac{dI_3}{dt} = k_9[DTT^{ox}][I_1] - k_{11}[DTT^{ox}][I_3] + k_7[DTT^{ox}][2S] \quad (14)$$

$$\frac{dN}{dt} = k_{10}[DTT^{ox}][I_2] + k_{11}[DTT^{ox}][I_3] \quad (15)$$

The concentrations of DTT^{ox} and DTT^{red}, for use in eqs 9−15, were obtained from the following equations:

$$[DTT^{ox}] = [DTT^{ox}]_{initial} - [DTT^{red}] \quad (16)$$

$$[DTT^{red}] = [DTT^{red}]_{initial} + [1S] + 2([2S] + [I_1]) + 3([I_2] + [I_3]) + 4[N] \quad (17)$$

The system of differential equations (eqs 9−15) was solved numerically by using the fourth-order Runge−Kutta method (*20*), requiring that the computed time-dependent curves for the evolution of each species provided a best fit to the experimental data. Thus, the best-fit redox-independent observed rate constants were determined by a simplex algorithm in conjunction with a modified Monte Carlo method to randomize the data sets before fitting (*21*). Random noise was generated by using a Box−Muller algorithm (*22*), which provides a Gaussian distribution of height 1 and standard deviation 1. Noise was included in the experimental values by adding a number chosen ran-

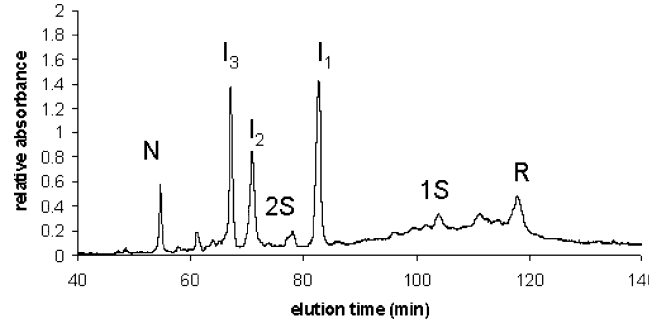

FIGURE 2: Example of an SCX−HPLC analysis of the distribution of AEMTS-blocked intermediate species from the oxidative folding of ONC after 90 min in 25 mM DTT^{ox} and 66 μM DTT^{red} at 25 °C and pH 8.0. The species were separated on a TOSOH Biosciences TSKgelTM SCX column (SP-5PW, 7.5 cm × 7.5 mm) using 25 mM HEPES and 3 mM EDTA as a running buffer (pH 8) and an NaCl gradient for separation. I_1, I_2, and I_3 have been identified as des-[19−68,30−75], des-[30−75], and des-[19−68], respectively (*14*).

Table 1: Observed Rate Constants for Each Step in the Oxidative Folding Mechanism (eqs 1−8) Determined at pH 8.0 and 25 °C

redox-independent rate constant	k (M^{-1} min^{-1})[a]	k (M^{-1} min^{-1})[b]
k_1	14.0 ± 0.14	18.0 ± 0.75
k_2	2770 ± 51	2600 ± 357
k_3	0.19 ± 0.01	0.20 ± 0.01
k_4	14 ± 4.3	20 ± 5
k_5	0.62 ± 0.01	0.63 ± 0.02
k_6	45 ± 7.5	50 ± 7
k_7	1.00 ± 0.07	1.0 ± 0.2
k_8	1.28 ± 0.02	1.25 ± 0.07
k_9	0.39 ± 0.03	0.41 ± 0.04
k_{10}	0.59 ± 0.01	0.65 ± 0.04
k_{11}	0.28 ± 0.01	0.22 ± 0.06

[a] Computed from the original experimental data. [b] Computed from the "experimental" data, created by varying the original k values to test their uniqueness.

domly from the generated Gaussian error distribution and multiplied by the experimentally determined standard deviation of that experimental value. By applying this procedure to each experimental value and thereby providing a Runge−Kutta solution for each value, we obtained 50 copies of each rate constant. An arithmetical average of each rate constant and its standard deviation resulted form this procedure. By analyzing these additional data sets, we improved the accuracy and precision of the k values.

To verify that the rate constants produced by this fitting procedure uniquely describe the time dependence of each of the species, a new set of "experimental" data was generated from a new set of k values, computed by changing each of the k values of column 2 of Table 1 by ±30%. The Runge−Kutta procedure was then applied to this new set of "experimental" data to compute a new set of k values (column 3 of Table 1). Both sets, listed in Table 1, are in agreement within standard deviations with the experimentally determined set, given that this test was performed for only one redox condition whereas the original set was obtained by combining the data from all the redox conditions that were examined.

As noted by Thannhauser and co-workers (*23*), the intermediate species can have different absorbtivities at 280 nm because the intermediates have varying degrees of structure that would affect the measured absorptivity. This effect was corrected by use of a plot of area under a peak versus concentration of a particular species, measured by NTSB analysis (*24*).

CD Spectra of the Structured Intermediates, I_1, I_2, I_3, and N. The extent of nativelike structure for the structured intermediates, I_1, I_2, and I_3, was determined by CD spectroscopy with an AVIV Biomedical (model 202-01) spectropolarimeter and compared to the CD spectrum of N. The mean residue ellipticity (MRE) was measured in the far-UV region, from 190 to 260 nm. Samples were prepared by populating the intermediates by oxidative folding to maximize the quantity of the intermediates (25 mM DTT^{ox} and 16 μM DTT^{red} at 25 °C and pH 8.0 for 90 min). Aliquots of the folding mixture were blocked with AEMTS and separated by SCX−HPLC as described in Oxidative Folding of ONC and SCX−HPLC Analysis. Each of the blocked intermediates was collected as it eluted off the column, and the pH of the collected fraction was adjusted to 3 with glacial acetic acid. The SCX−HPLC buffer salts and NaCl from each intermediate were removed by RP-HPLC as described in Oxidative Folding of ONC and SCX−HPLC Analysis. Water, acetonitrile, and TFA were removed by lyophilization, and the intermediates were each reconstituted in 50 mM acetic acid to be analyzed by CD spectroscopy at pH 3.0. This pH was chosen to avoid removal of the blocking groups during the CD measurements because the disulfide bond between the protein moiety and the blocking group is more stable at a low pH (*25*). The CD spectrum of 50 mM acetic acid was subtracted from the CD spectra of the protein solutions. To convert the observed circular dichroism signal from millidegrees to MRE, the concentration of each of the solutions had to be measured accurately. The concentration of each solution was determined by thiolate analysis utilizing NTSB and sulfite reduction of disulfides, as described in ref *24*. The disulfide content of each intermediate was obtained from the additional thiols resulting from sulfite reduction of its disulfide bonds (*24*). Each of the intermediates has a different number of thiols produced by reduction of intramolecular disulfide bonds and of the disulfide bonds produced by covalent attachment of the thiols to the blocking group, $-SCH_2CH_2NH_3^+$. I_1 has 12 free thiols (four from the two S−S bonds, four from the free thiols blocked with AEMTS, and four from the cystamine group of the released blocking group, $-SCH_2CH_2NH_3^+$). I_2 and I_3 each have 10 free thiols (six from the three S−S bonds, two from the free thiols blocked with AEMTS, and two from the cystamine group of the released blocking group, $-SCH_2CH_2NH_3^+$). N has eight free thiols (eight from the four S−S bonds). After CD spectra were obtained for all of the blocked intermediates and N-ONC, they were checked by SCX−HPLC to ensure that the disulfide bonds of each of the species did not undergo possible removal of the blocking group with attendant SH/S−S reshuffling. This SCX−HPLC method for analyzing AEMTS-blocked species is sufficient for testing these side reactions because it can separate species that have the same number of disulfide bonds, I_2 and I_3, and species that contain different numbers of disulfide bonds, which would have a different number of blocking groups, $-SCH_2CH_2NH_3^+$, that give rise to different cationic affinities.

Thermal Stability of AEMTS-Blocked Intermediates I_1, I_2, I_3, and N. Thermal denaturation of AEMTS-blocked I_1, I_2, I_3, and N was monitored by CD spectroscopy, and samples were prepared as described in the previous section. The percent of folding was monitored by CD at 198 nm, the wavelength at which there was the greatest difference between the folded and unfolded spectra. The temperature range studied was from 25 to 97.5 °C. The temperature was changed in increments of 5 °C in the range corresponding to folded and unfolded species, 2.5 °C as the folding transition approached, and 1 °C during the folding transitions. Each solution was equilibrated to keep the temperature within 0.1 °C for 2 min before data were collected for 60 s. The corresponding error in the CD (0.8 mdeg) was observed to be maintained for 5 min of temperature equilibration and 5 min of data collection. Heating and cooling curves were obtained to show reversibility of the denaturation process. After each thermal unfolding experiment, the sample was checked by SCX−HPLC to ensure that the disulfide bonds of the species did not reshuffle.

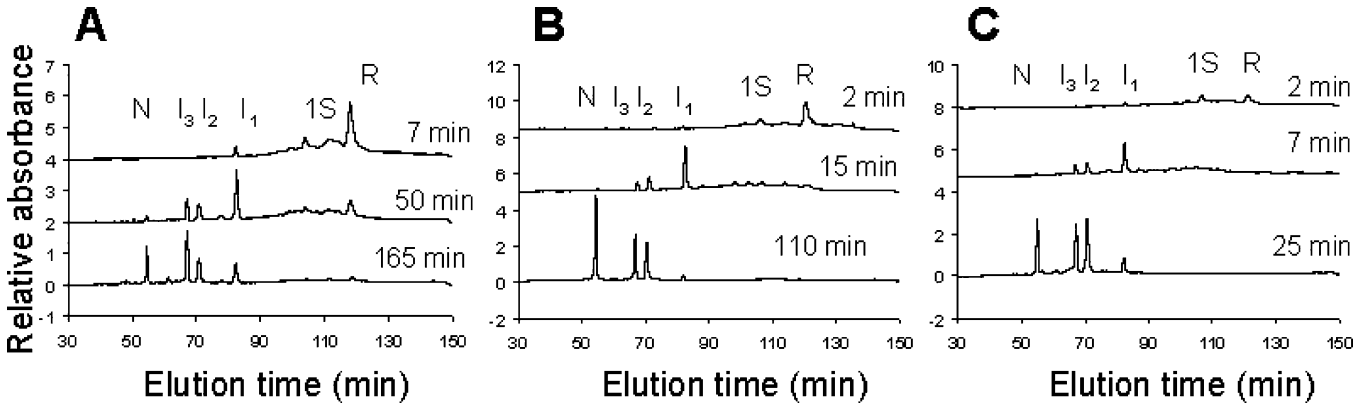

FIGURE 3: Different distributions of intermediate species under different conditions: (A) 25 mM DTT^{ox} and 66 μM DTT^{red} at pH 8.0 and 25 °C 7, 50, and 165 min into the oxidative folding process, (B) 25 mM DTT^{ox} without DTT^{red} at pH 8.0 and 25 °C 2, 15, and 110 min into the oxidative folding process, and (C) 70 mM DTT^{ox} without DTT^{red} at pH 8.0 and 25 °C 2, 7, and 25 min into the oxidative folding process.

The thermal denaturation curves were fit to a two-state model, and thermodynamic parameters were extracted by the following equations:

$$\Delta G_{unf} = -RT \ln\left(\frac{f_u}{f_f}\right) \quad (18)$$

$$\Delta G_{unf} = \Delta H_{unf} - T\Delta S_{unf} \quad (19)$$

$$T_m = \Delta H_{unf}/\Delta S_{unf} \text{ at } \Delta G_{unf} = 0 \quad (20)$$

RESULTS

The separation of intermediate blocked species at different reaction times and different elution times is shown for three redox conditions in panels A, B, and C of Figure 3. The relative populations of each of the intermediate species in chromatograms of this type were obtained quantitatively by integrating the area under curves produced from each of the intermediates. It was observed that the elution times of the intermediates are very reproducible, and the assignment of a consistent baseline for integration of peak area could be obtained by superimposing each of the corresponding chromatograms. Analysis of the relative changes in populations for each intermediate species, by Runge−Kutta solutions for the system of eqs 9−15, for oxidative folding reactions under a variety of redox conditions, led to the oxidative folding mechanism of eqs 1−8, shown in Figure 4, which provided the best fit to the experimental data. The time dependencies of the various species are shown in Figure 5 for two oxidizing conditions, 25 mM DTT^{ox} and 70 mM DTT^{ox}. The observed rate constants that correspond to each of the steps in the mechanism over the entire redox range are presented in column 2 of Table 1.

The oxidative folding of ONC is much faster than that of RNase A. According to previous work (*2*), 60% of RNase A is recovered in 400 min in the presence of 100 mM DTT^{ox} and 16 μM RNase A. However, 80% of ONC is recovered in 95 min in the presence of 70 mM DTT^{ox} and 17 μM ONC. The following analysis of the kinetic and thermodynamic role of various structured and unstructured species involved in the oxidative folding of ONC provides insight into the more efficient folding of ONC.

Kinetic Mechanism: Unstructured Ensembles. The 1S and 2S peaks in the chromatogram in Figure 2 were identified as having one- and two-disulfide species by mass spectrometry and as unstructured (*14*) because they did not survive a reduction pulse before being blocked with AEMTS. By the same criterion, I_1, I_2, I_3, and N are structured.

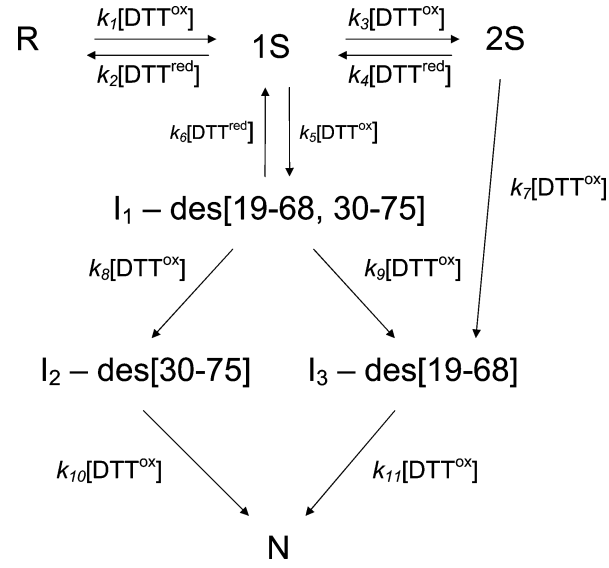

FIGURE 4: Oxidative folding mechanism for ONC. No 3S or 4S ensembles were detected under all of the oxidative folding conditions. The only three-disulfide-bond species are I_2 and I_3, and the only four-disulfide-bond species is N.

As shown in Figure 3, the first step in the oxidative folding of R-ONC by DTT^{ox} is the formation of an unstructured ensemble of species containing one disulfide bond (1S). This ensemble elutes right before R-ONC on the chromatogram and does not consist of a single peak. Rather, the number of peaks corresponds to different 1S species eluting at different times, 95−118 min, as seen in panels A, B, and C of Figure 3. In the mechanism in Figure 4, there is a pre-equilibrium between R-ONC and the 1S ensemble, between the 1S and 2S ensembles, and between the 1S ensemble and I_1. The observed rate constants for oxidation and reduction of the 1S and 2S ensembles do not correspond to those of a single-disulfide species; each member of the ensemble contributes to the observed rate constant. To take into account the possible number of species in each ensemble to obtain the intrinsic rate constant for each species in the ensemble, the observed rate constants are modified by inclusion of appropriate statistical factors, as shown in Table 2. For the

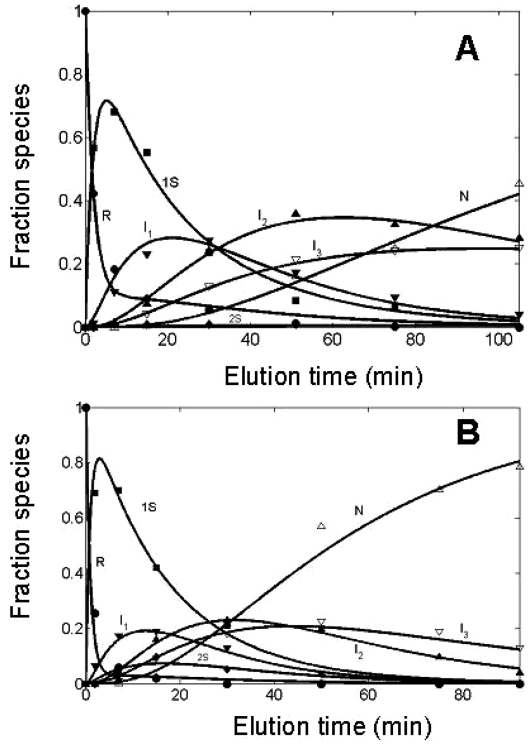

FIGURE 5: Changes in the distribution of species (R-ONC, 1S, 2S, I_1, I_2, I_3, and N-ONC) over time, fit to the oxidative folding mechanism shown in Figure 4. The condition analyzed in panel A was 25 mM DTT^{ox} at 25 °C and pH 8.0, and that in panel B was 70 mM DTT^{ox} at 25 °C and pH 8.0.

Table 2: Modified Rate Constants[a] Involved in Unstructured Ensembles at 25 °C and pH 8.0

	k_f[b]	k_f^{ave}[c]	k_{intra}[d]	k_r[b]	k_r^{ave}[c]
k_1	14	0.5	70.9	–	–
k_2	–	–	–	2770	2770
k_3	0.19	0.013	1.84	–	–
k_4	–	–	–	14	7

[a] In units of M^{-1} min^{-1}. [b] k_f and k_r refer to observed rate constants for oxidation and reduction steps, respectively. k_1 and k_3 correspond to oxidations of R and 1S, respectively, while k_2 and k_4 correspond to reductions of 1S and 2S, respectively. [c] k_f^{ave} and k_r^{ave} are modified for statistical factors that arise from the oxidation or reduction of each member of the respective ensembles to give the average rate among all of the members of the ensembles. For k_1, there are 28 different ways to form the 1S ensemble from R, and therefore, k_1 is divided by 28. For k_3, there are 15 ways to form the 2S ensemble from any member in the 1S ensemble, and therefore, k_3 is divided by 15. In a similar manner for the rate constants corresponding to reductions, k_2 is not corrected because there is only one way to form R from any member of the 1S ensemble. k_4 is divided by 2 because there are two ways of forming a 1S species from any member of the 2S ensemble. [d] k_{intra} is a rate constant (in min^{-1}) for a redox-independent, intramolecular disulfide reshuffling step during the oxidation of a disulfide bond using DTT^{ox}. It is determined by using the value 7.05×10^{-3} M^{-1} for K_{DTT} (*23, 26*) in eq 22, as discussed in the text.

unstructured ensembles, 1S and 2S, the magnitudes of these modified rate constants are different, namely, 0.5 and 0.013 for the oxidation to form 1S and 2S, respectively, and 2770 and 7 for the reduction of 1S and 2S, respectively. The different modified rate constants reflect the different intrinsic reactivities of the members of each of the unstructured ensembles. However, according to ref *2*, the modified rate constants of RNase A are similar in magnitude for the oxidation and reduction of the 1S, 2S, 3S, and 4S ensembles, which indicates that the free energy barriers of each step are the same. Therefore, while there is still no nativelike structure in these ensembles, the different free energy barriers in ONC reflect different interactions in the unfolded state of ONC compared to RNase A.

Another quantity that helps characterize the interactions in these unstructured ensembles is k_{intra}. k_{intra} is a redox-independent rate constant that reflects the relative rate of intramolecular SH/S−S reshuffling. The reshuffling process in the oxidation of two cysteines to form a disulfide bond is characterized by the following steps:

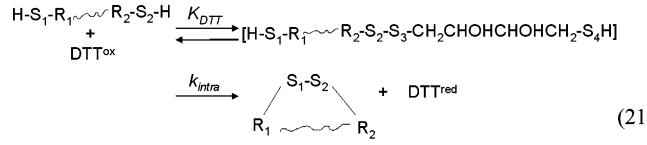

(21)

First, $H\text{-}S_1\text{-}R_1R_2\text{-}S_2\text{-}H$ forms an unstable mixed disulfide with DTT^{ox} to a degree determined by K_{DTT}. The value of K_{DTT} has been derived previously (*26*) and is 7.05×10^{-3} M^{-1}. S_4 could react with S_3 to regain a molecule of DTT^{ox}, or S_1 could attack S_2 with a rate constant k_{intra} to release a molecule of DTT^{red} and leave S_1 and S_2 in a disulfide bond; i.e., S_4 of the dithiothreitol moiety could release $H\text{-}S_1\text{-}R_1R_2\text{-}S_2\text{-}H$ and regain a molecule of free DTT^{ox}, or S_1 can attack S_2 at a rate of k_{intra} to release a molecule of DTT^{red} and leave S_1 and S_2 oxidized. k_{intra} can be computed with the equation

$$k_f^{ave} = K_{DTT}k_{intra} \quad (22)$$

where k_f^{ave} is an intrinsic rate constant, obtained from the observed k values of Table 1 for oxidation reactions, modified by statistical factors, similarly for k_r^{ave}. Values for k_{intra} are shown for the 1S and 2S ensembles in Table 2.

In the context of the oxidative folding pathway, the observed oxidation or reduction rate constants, k_f or k_r, respectively, can be multiplied by the concentration of DTT^{ox} or DTT^{red}, respectively, used in these experiments and compared to the rate of intramolecular reshuffling reactions. In all reactions, the rate of reshuffling (in terms of k_{intra}) for either species is 10^2-10^3 times larger than the average rate of oxidation or reduction. This indicates that the individual species of the 1S and 2S ensembles reshuffle fast enough to treat these ensembles as a single kinetic entity.

Under all conditions, with an example shown in Figure 5, the concentration (calculated with the observed rate constants of Table 1 together with the concentrations of DTT^{ox}) of I_1 is always greater than that of 2S. This is consistent with the mechanism of Figure 4 in which the pathway from I_1 to N (through I_2 and I_3) is favored over the pathways from 2S to ONC (through I_3).

One interesting omission from the mechanism for oxidation of ONC [different from that of RNase A (*2*)] is the absence of unstructured ensembles containing three and four disulfide bonds (3S and 4S). To verify the omission of these species in the mechanism of Figure 4, it was necessary to identify the chromatographic elution times of 3S and 4S ensembles of ONC, in which the concentration of N is very small. For this purpose, GdnHCl was added to R-ONC in an oxidative-folding experiment. The resulting chromatogram in Figure 6A shows the elution pattern of 3S and 4S. On the other hand, in the absence of GdnHCl, no 3S or 4S peaks appear during oxidative folding. By avoiding 3S and 4S

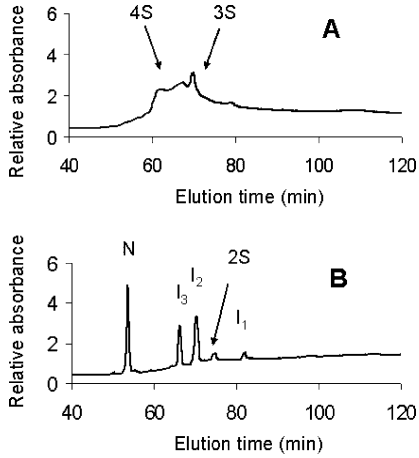

FIGURE 6: (A) Elution of the 3S and 4S ensembles that were populated by performing oxidative folding with 115 mM DTT^{ox} at 25 °C and pH 8.0 in the presence of GdnHCl. (B) Oxidative folding without GdnHCl under the same redox condition. No 3S or 4S ensemble is observed under this condition.

ensembles, which would have non-native interactions, ONC can explore conformational space more efficiently than RNase A does.

Kinetic Mechanism: Structured Intermediates. A critical step in the oxidative folding mechanism of ONC is the formation of structured intermediate I_1, des-[19−68,30−75], which (along with I_2, I_3, and N) is identified as one that survives a reduction pulse (*14*), applied to the oxidation mixture. Once I_1 is formed, two of four native disulfide bonds are in place, and from this intermediate, the remaining native disulfide bonds are formed in I_2, des-[30−75], and I_3, des-[19−68], and finally in N. In Figure 5, I_2 and I_3 can be observed forming after I_1 is populated. Under both conditions in Figure 5, I_2 is preferentially formed over I_3 at the same concentration of DTT^{ox} as indicated by its more rapid rate of formation ($k_8 > k_9$). The decays of I_2 and I_3 are also different. The more rapid decay of I_2 relative to that of I_3 ($k_{10} > k_{11}$) under both conditions in Figure 5 indicates that I_2 is more readily oxidized to N than I_3 at the same concentration of DTT^{ox}. For the formation and oxidation of I_2, the observed rate constants corresponding to these two steps are larger for I_2. In the next section, the importance of I_2 at different temperatures is discussed. Similar relative reactivity between these structured intermediates is observed when oxidative folding to form native ONC is initiated from unblocked I_1; I_2, I_3, and N are formed by oxidation of I_1 with DTT^{ox}, as shown in Figure 7. The amount of I_2 present at the beginning is due to the overlapping of the I_1 and I_2 peaks during the preparative separation of I_1 by RP-HPLC.

An interesting observation about the formation and further oxidation of I_1, seen under both conditions in Figure 5, is that the rate of formation of I_1 in a bimolecular reaction from a relatively high concentration of an unstructured ensemble (1S) is faster than the rate of further oxidation of a relatively lower concentration of I_1 compared to 1S to form I_2 and I_3. RNase A exhibits the opposite behavior in that its first structured species, des-[40−95] and des-[65−72] (*1, 2*), appear more slowly in a unimolecular reshuffling rate-determining step than its more rapid oxidation in a bimolecular step to N. As a result, the observed populations of these structured species in RNase A are very small because, once they are formed in the rate-determining steps,

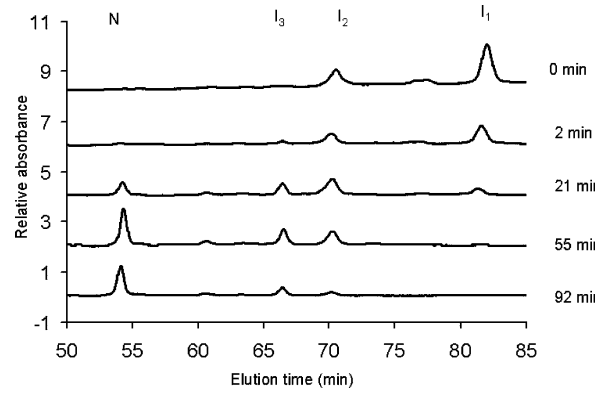

FIGURE 7: Oxidation of unblocked I_1 at 70 mM DTT^{ox}, 25 °C, and pH 8.0. I_2 is also present at the beginning of the oxidation because it eluted close to I_1 during its preparation by RP-HPLC. As I_1 is being oxidized, N, I_3, and more I_2 are also formed as oxidation proceeds.

they are subsequently oxidized very rapidly. Because of the rapid formation of I_1 in ONC and its slower subsequent oxidation, the structured intermediates dominate the population of intermediate species during the folding pathway and play a greater role in the oxidative folding mechanism.

Effects of Temperature on the Oxidative Folding Pathway. The oxidative folding of ONC was studied at various temperatures, from 15 to 57 °C (Table 3), to identify the key steps that drive the formation of structure. Were oxidative folding to be performed at higher temperatures, the less stable species would be destabilized and only the more stable ones would drive the folding. The effects of different temperatures on the recovery of ONC are shown in Figure 8. Aside from the decrease in rate between 15 and 25 °C, the rate of formation of N increases with temperature until 47 °C, and at 57 °C, the rate decreases because of thermal destabilization of intermediate species such as the 1S ensemble and I_1.

The rate of formation of N decreases as the temperature increases from 15 to 25 °C because undetermined interactions in R and/or 1S are stabilized at the lower temperature, as indicated by considering the following equilibrium:

$$R + 2DTT^{ox} \overset{k}{\rightleftarrows} I_1 + 2DTT^{red} \tag{23}$$

with equilibrium constant

$$K = \left(\frac{k_1}{k_2}\right)\left(\frac{k_5}{k_6}\right) \tag{24}$$

The value of K decreases from 0.0024 at 15 °C to 7.0×10^{-5} at 25 °C and increases to 0.0013 at 37 °C. Even though K is lower at 37 °C than at 15 °C, the greater rate of formation of N at 37 °C is due to the larger rate constant, k_8, at 37 °C compared to that at 15 °C, by a factor of 10 for the formation of I_2 from I_1 (also, see Figure 9).

At temperatures higher than 37 °C, the distribution of species changes so that only species that are stable at higher temperatures are populated to recover N-ONC. At these temperatures, these fewer species fold faster.

The oxidation of I_1 to form I_2 (with rate constant k_8) preferentially over I_3 (with rate constant k_9) is observed in the formation of N-ONC at higher temperatures (Table 3). Rate constants k_8 and k_9 refer to the oxidation of I_1 to I_2 and

Table 3: Observed Rate Constants for Each Step in the Oxidative Folding Mechanism at Different Temperatures at pH 8.0

	k (M^{-1} min^{-1})				
	15 °C	25 °C	37 °C	47 °C	57 °C
k_1	26 ± 1.3	14.0 ± 0.14	26 ± 2.2	40.0 ± 0.8	53.0 ± 0.46
k_2	160 ± 43	2770 ± 51	6800 ± 782	−	−
k_3	0.67 ± 0.01	0.19 ± 0.01	−	−	−
k_4	70 ± 15	14 ± 4.3	−	−	−
k_5	1.94 ± 0.04	0.62 ± 0.01	0.83 ± 0.01	14.0 ± 0.20	3.10 ± 0.01
k_6	130 ± 34	45 ± 7.5	2 ± 1.8	−	−
k_7	4.70 ± 0.9	1.00 ± 0.07	−	−	−
k_8	1.08 ± 0.08	1.28 ± 0.02	12 ± 1.6	85.00 ± 0.01	78.00 ± 0.01
k_9	1.15 ± 0.03	0.39 ± 0.03	0.3 ± 0.12	−	−
k_{10}	0.64 ± 0.03	0.59 ± 0.01	2.2 ± 0.3	5.80 ± 0.09	5.90 ± 0.01
k_{11}	0.24 ± 0.03	0.28 ± 0.01	18.0 ± 0.8	−	−

I_3, respectively. From 15 to 47 °C, the ratio k_8/k_9 increases considerably, favoring the formation of I_2 relative to I_3.

Thermodynamic Stability of Intermediates I_1, I_2, I_3, and N. The extent of global folding of I_1, I_2, I_3, and N was determined by far-UV circular dichroism spectroscopy, a probe for secondary structure. The spectra, shown in Figure 10, are compared to that of unfolded species R-ONC. Each of the intermediates is observed to have a degree of nativelike structure as indicated by the maxima at 198 nm and the broad minima from 208 to 222 nm. Even the two-disulfide-bond intermediate, I_1, contains a substantial amount of secondary structure. The broad minima from 208 to 222 nm for the intermediates are not as substantial, compared to N-ONC, which indicates that there is only partial native structure.

To measure the thermodynamic stability of these partially folded intermediates, temperature denaturation experiments were carried out by monitoring the loss of structure at 198 nm. The results are shown in Figure 11. The solid characters were used to extract thermodynamic data, and the unfilled characters show heating and cooling curves to demonstrate reversibility. The remarkable stability of ONC can be observed when thermodynamic data for ONC are compared with existing thermodynamic data for RNase A (*12, 13, 27, 28*). The results are summarized in Table 4. Essentially, the three-disulfide-bond intermediates in ONC (I_2 and I_3) at pH 3.0 are as stable ($\Delta G_{unf} \sim 10$ kcal mol^{-1}) as native RNase A at pH 4.6 with four disulfide bonds. The two-disulfide-bond intermediate, I_1, at pH 3.0 in ONC is as stable as the three-disulfide-bond intermediates in RNase A at pH 4.6 as indicated by similar magnitudes of their melting temperatures, T_m, and their free energies of unfolding. The stability of RNase A decreases when the pH is reduced from 4.6 to 3.0 (*28*).

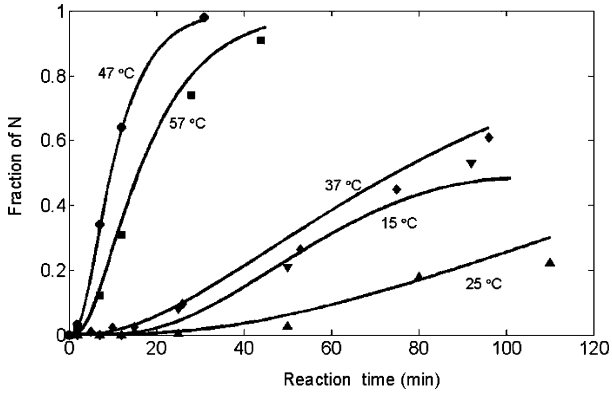

FIGURE 8: Recovery of N-ONC at different temperatures, 15, 25, 37, 47, and 57 °C, at pH 8.0 (25 mM DTT^{ox} and 16 μM DTT^{red}).

The free energy of unfolding, ΔG_{unf}, was calculated from eq 18, with the terms f_u and f_f determined from the CD signal, compared to the CD signals for the folded and unfolded protein, at each temperature. With a plot of ΔG_{unf} against T, $-\Delta S_{unf}$ and ΔH_{unf} were evaluated as the slope and intercept, respectively, of this plot. The transition temperature, T_m, was evaluated as the temperature at which $\Delta G_{unf} = 0$ (eq 20).

DISCUSSION

Comparison of Oxidative Folding Rates of ONC and RNase A. The oxidative folding of ONC to recover its biologically active form is faster than that of its structural

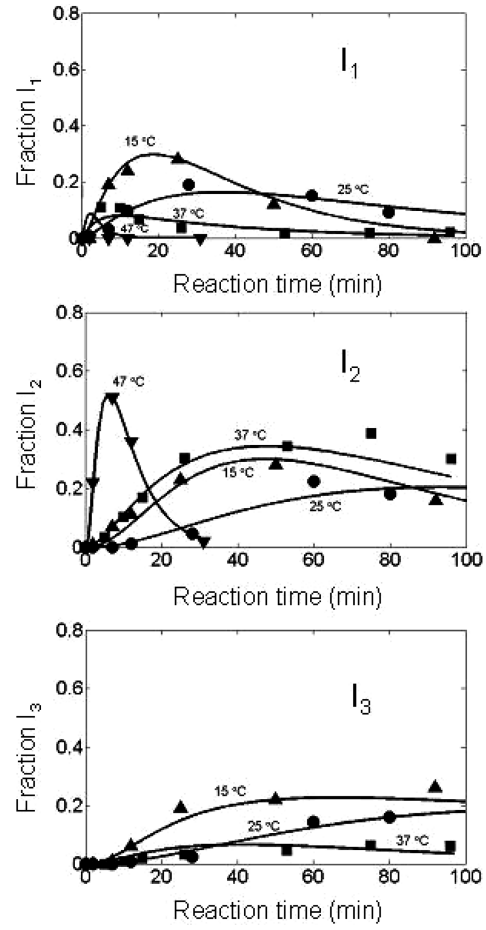

FIGURE 9: Kinetic fate of the structured intermediates at different temperatures [15 (▲), 25 (●), 37 (■), and 47 °C (▼)] under the same conditions as in Figure 8. Corresponding observed rate constants are listed in Table 3. As the temperature is increased, I_1 becomes more reactive to DTT^{ox} and is oxidized to I_2 faster than to I_3 to form N-ONC. I_1 and I_3 are populated to a very low extent at higher temperatures.

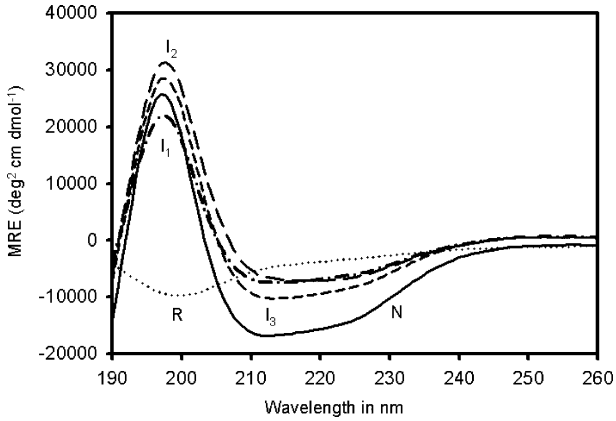

FIGURE 10: Far-UV CD spectra of different species populated along the oxidative folding pathway at 25 °C and pH 3.0: R, unblocked R-ONC; I_1, AEMTS-blocked; I_2, AEMTS-blocked; I_3, AEMTS-blocked; N, N-ONC.

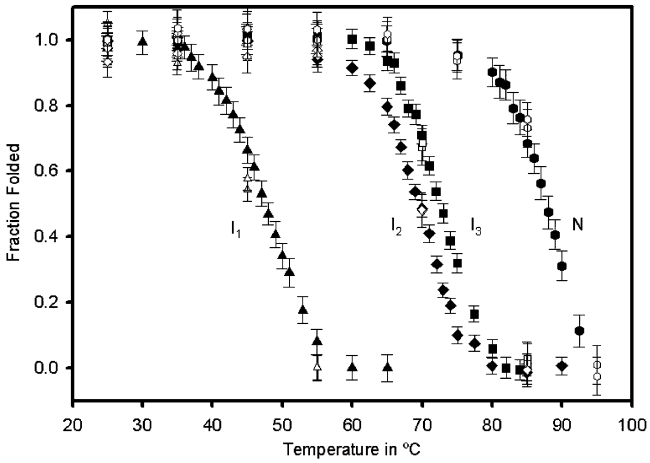

FIGURE 11: Temperature denaturation at pH 3.0 of different species populated along the oxidative folding pathway: I_1, AEMTS-blocked (▲); I_2, AEMTS-blocked (◆); I_3, AEMTS-blocked (■); N, N-ONC (●). Unfilled characters correspond to heating and cooling curves of each of the species.

Table 4: Thermodynamic Data Obtained from Temperature Denaturation of Each Species and Compared to Similar Data for RNase A

	T_m (°C)	ΔG_{unf} (kcal mol^{-1} at 25 °C)
WT RNase A	47[a]	3[a]
WT RNase A	56 ± 0.2[b]	10.7 ± 0.2[b]
des-[65−72]−RNase A	39 ± 0.2[c]	3.5 ± 0.4[c]
des-[40−95]−RNase A	34 ± 0.2[d]	2.0 ± 0.1[d]
WT ONC	94 ± 4.4[e]	14.0 ± 0.5[e]
I_1−des-[19−68,30−75]−ONC	45 ± 2.6[e]	4.1 ± 0.2[e]
I_2−des-[30−75]−ONC	71 ± 3.5[e]	9.8 ± 0.9[e]
I_3−des-[19−68]−ONC	76 ± 7.7[e]	9.5 ± 0.8[e]

[a] From ref *28*, at pH 3.0. [b] From ref *12*, at pH 4.6. [c] From ref *12*, performed on [C65S,C72S] at pH 4.6. [d] From ref *13*, performed on [C40A,C95A] at pH 4.6. [e] At pH 3.0.

homologue, RNase A. By avoiding formation of 3S and 4S ensembles, present in RNase A, ONC can explore conformational space more efficiently. This could be facilitated by interactions which lead to very stable intermediates compared to those of RNase A. These interactions could also account for the preferential populations of key species at higher temperatures, such as I_1 and I_2 (Figure 9).

Another aspect of the more efficient folding mechanism of ONC is the presence of a two-disulfide-bond intermediate, I_1. While it is not as stable as a three-disulfide-bond species, it aids in attaining three-disulfide bond intermediates (I_2 and I_3) from an unstructured 1S ensemble. In RNase A, the structured species, des-[40−95] and des-[65−72], are populated from a 3S ensemble by a reshuffling reaction. In ONC, by utilizing a 1S → I_1 → I_2 + I_3 pathway, the search for a structured species (I_1) from an unstructured ensemble involves roughly 15 times fewer species; i.e., rather than searching for two species out of 420 theoretical ones in the 3S ensemble of RNase A, the structured species, I_1 in ONC, is formed by oxidation of either of two 1S species out of 28 theoretical ones. In addition, the native disulfide bonds in I_1 are [87−104] and [48−90]. The [87−104] disulfide bond connects the shortest portion of the peptide chain and, thus, incurs the lowest entropic penalty in loop formation of ONC compared to the other disulfide bonds. Also, there are hydrophobic contacts among residues 86−104 (with hydrophobic residues in boldface type, **f**c**v**tcenqap**v**h**f**v**g**v**g**sc) at the C-terminus that could possibly form stable contacts without the need for a disulfide bond (*29*). In RNase A, the [65−72] disulfide bond is the first one to form, despite the fact that within this loop there are no hydrophobic residues. The non-native disulfide bond, [58−65], with a similar loop size, is also populated in the early stages of oxidative folding (*4*), but not to the same extent as the [65−72] disulfide bond. Both of these disulfide bonds form the same size loop, so presumably, the favorable enthalpic interactions in the native [65−72] disulfide loop account for why this disulfide bond is preferred in a ratio of 4:1 (*4*) in the oxidative folding pathway over the [58−65] disulfide bond.

Table 5: Rate of Oxidative Folding of RNase A at Different Temperatures at pH 8.0, Obtained from ref *11*

k ($\times 10^4$ min^{-1})[a]	T (°C)
7.2 ± 0.5	15
12.5 ± 0.6	25
1.3 ± 0.2	37

[a] The rate of oxidative folding of RNase A can be approximated by a first-order rate equation, ln[1-N] = $-kt$, to which these rate constants correspond.

In addition, these nonpolar residues could be responsible for the hydrophobic stabilization at higher temperatures, and the increase in folding rate above 25 °C, in contrast to the decrease observed in RNase A (Table 5). In RNase A, the oxidative folding rate slows as the temperature is increased. It is known that hydrophobic interactions are stabilized as the temperature increases (*30*−*32*).

Other hydrophobic interactions could also influence the preferential oxidation of I_1 to I_2 over I_3 at elevated temperatures. To form I_2 from I_1, residues Cys19 and Cys68 must be oxidized to form the [19−68] disulfide bond, and to form I_3 from I_1, residues Cys30 and Cys75 must be oxidized to form the [30−75] disulfide bond. Therefore, the preference to form I_2 or I_3 is based on the penalty of forming or not forming the [19−68] or [30−75] disulfide bond, respectively. The [19−68] disulfide bond is buried with other hydrophobic residues, according to the structure in Figure 1. However, the [30−75] disulfide bond is almost 4 times more exposed than the other disulfide bonds in RNase A (*33*). Therefore, at higher temperatures, stronger hydrophobic tendencies could be responsible for oxidizing Cys19 and Cys68 instead of Cys30 and Cys75.

Table 6: Free Energy Penalty, ΔG_U, from Formation of a Disulfide Bond Calculated from Theory and Compared to Experiment

	ΔS_x[a] (kcal mol^{-1} K^{-1})
I_1	−0.033
I_2	−0.050
I_3	−0.051
N	−0.065

	ΔG_U (kcal mol^{-1})	
loop formation	theoretical value[b]	experimental value[c]
I_1 to I_2 at 60 °C	5.69	5.11 ± 0.8
I_1 to I_3 at 60 °C	5.99	6.01 ± 0.8
I_2 to N at 80 °C	5.29	4.87 ± 0.9
I_3 to N at 80 °C	4.94	3.97 ± 0.9
I_1 to N at 60 °C	10.66	10.18 ± 0.5

[a] Theoretical calculation of the entropy loss due to loop closure for each intermediate according to ref *34*. [b] Theoretical $\Delta G_U = -T\Delta\Delta S_x$ at 60 or 80 °C and $\Delta\Delta S_x$ according to the loop formation indicated. [c] Experimental ΔG_U for each loop formation according to the following equations: $\Delta G_U = [\Delta G_{unf}(<0)_{I_2 \text{ or } I_3} - \Delta G_{unf}(<0)_{I_1}]$ at 60 °C for I_1 to I_2 or I_3, $\Delta G_U = [\Delta G_{unf}(>0)_N - \Delta G_{unf}(<0)_{I_2 \text{ or } I_3}]$ at 80 °C for I_2 or I_3 to N, and $\Delta G_U = [\Delta G_{unf}(>0)_N - \Delta G_{unf}(<0)_{I_1}]$ at 60 °C for I_1 to N.

Role of Disulfide Bonds in Stabilizing Intermediates. After considering the thermodynamic stability of the structured intermediates and N-ONC, the origin of the increased stability can be ascribed to the entropy of formation of overlapping loops (*34*) by eq 23

$$\Delta S_x = R(-3.47m + 3m \ln a - 1.5 \ln|C|) \qquad (25)$$

where m is the number of disulfide-bonded loops in a particular species of ONC, a is the length of a chain element, and $|C|$ is the determinant of a matrix whose elements depend on the size of the overlapping loops. If the addition of the disulfide bond does not affect the three-dimensional structure of the folded state of a species, then the addition of the disulfide bond stabilizes the protein by decreasing the entropy of the unfolded state. The extent to which the unfolded state is destabilized ($\Delta G_U = \Delta\Delta G_{unf}$) can be taken as the difference between the free energy of unfolding of a protein with a disulfide bond and the free energy of unfolding of a protein without the disulfide bond. The temperature at which this difference is calculated must be chosen so that one protein is completely unfolded and the other is completely folded at this temperature.

This observed destabilization free energy, ΔG_U, can be compared to the calculated destabilization free energy by multiplying the differences in the entropy loss due to disulfide bond formation of two species, $\Delta\Delta S_x$, by the same temperature to obtain a theoretical free energy of unfolding. The calculated destabilization entropy, ΔS_x, of each of the structured intermediates, I_1, I_2, I_3, and N, was calculated and is listed in Table 6. These values of ΔS_x were used to compute $\Delta\Delta S_x$ which, multiplied by the appropriate T from Figure 11, led to the calculated values of ΔG_U listed in Table 6. These calculated destabilization free energies were compared to the observed destabilization free energies for these transitions.

Comparison of the calculated and observed destabilization free energies, ΔG_U, of Table 6 indicates that the stability of each of the intermediates relative to I_1 is due mostly to the entropic destabilization of the unfolded state of I_1, I_2, and I_3 by the addition of a disulfide bond. In other words, I_1 has a substantial amount of nativelike structure which is further stabilized by the addition of native disulfide bonds of I_2, I_3, and N. Therefore, the formation of I_1 plays an important part in stabilization of the native structure in ONC because most of the necessary interactions for the formation of the biologically active structure have already formed in I_1. The folding mechanism of ONC is contingent upon formation of structured species that oxidize to N and formation of an intermediate early in the oxidative folding mechanism that contains the necessary structure to obtain the biologically active form. Therefore, the oxidative folding pathway of ONC becomes more efficient than that of RNase A.

CONCLUSIONS

This study has demonstrated how the oxidative folding mechanism of ONC is different from that of RNase A, a structural homologue. ONC is more efficient at recovering biologically active structure than RNase A. ONC has more stabilizing interactions that restrict the conformational search to 1S and 2S ensembles without including the unstructured 3S and 4S ensembles, which would increase the number of non-native disulfide bonds. The cysteines that form the [87−104] and [48−90] disulfide bonds in I_1 are most likely aligned by hydrophobic interactions, as seen in the crystal structure. Further evidence for the importance of these hydrophobic interactions is the observation that the rate of folding increases with temperature as a combination of increasing reaction rate with temperature and an increased level of stabilization of hydrophobic interactions. At higher temperatures, intermediate I_2 is preferentially formed over I_3 presumably because of the hydrophobic residues surrounding Cys19 and Cys68 in I_1, which drive their oxidation. The addition of disulfide bonds also provides additional stability by decreasing the entropy in the unfolded state. Most of the native structure in N is formed in I_1, and biologically active stability is obtained for N via destabilization of the unfolded state of I_1 with native disulfide bonds. From this kinetic and thermodynamic study of the oxidative folding of ONC, we have learned that the sequence of ONC, when compared to that of RNase A, exhibits increased folding efficiency and thermodynamic stability. This comparison of two structurally homologous proteins shows how sensitive protein-folding mechanisms are to details of the amino acid sequence.

ACKNOWLEDGMENT

We thank R. J. Youle for providing the cDNA of ONC and B. R. Crane for access to his CD spectrometer.

REFERENCES

1. Rothwarf, D. M., Li, Y.-J., and Scheraga, H. A. (1998) Regeneration of bovine pancreatic ribonuclease A: Identification of two nativelike three-disulfide intermediates involved in separate pathways. *Biochemistry 37*, 3760–3766.
2. Rothwarf, D. M., Li, Y.-J., and Scheraga, H. A. (1998) Regeneration of bovine pancreatic ribonuclease A: Detailed kinetic analysis of two independent folding pathways. *Biochemistry 37*, 3767–3776.
3. Leland, P. A, and Raines, R. (2001) Cancer chemotherapy: Ribonucleases to the rescue. *Chem. Biol. 8*, 405–413.
4. Xu, X., Rothwarf, D. M., and Scheraga, H. A. (1996) Nonrandom distribution of the one-disulfide intermediates in the regeneration of ribonuclease A. *Biochemistry 35*, 6406–6417.
5. May 28, 2008, Press Release, http://www.ir-site.com/alfacell/press.html.

6. Arnold, U., and Ulbrich-Hofmann, R. (2006) Natural and engineered ribonucleases as potential cancer therapeutics. *Biotechnol. Lett. 28*, 1615–1622.
7. Ardelt, W., Shogen, K., and Darzynkiewicz, Z. (2008) Onconase and amphinase, the antitumor ribonucleases from *Rana pipiens* oocytes. *Curr. Pharm. Biotechnol. 9*, 215–225.
8. Notomista, A., Catanzano, F., Graziano, G., Dal Piaz, F., Barone, G., D'Alessio, G., and Di Donato, A. (2000) Onconase: An unusually stable protein. *Biochemistry 39*, 8711–8718.
9. Lee, J. E., and Raines, R. (2003) Contribution of active-site residues to the function of onconase, a ribonuclease with antitumoral activity. *Biochemistry 42*, 11443–11450.
10. Rothwarf, D. M., and Scheraga, H. A. (1993) Regeneration of bovine pancreatic ribonuclease A. 1. Steady-state distribution. *Biochemistry 32*, 2671–2679.
11. Rothwarf, D. M., and Scheraga, H. A. (1993) Regeneration of bovine pancreatic ribonuclease A. 4. Temperature dependence of the regeneration rate. *Biochemistry 32*, 2698–2703.
12. Shimotakahara, S., Rios, C. B., Laity, J. H., Zimmerman, D. E., Scheraga, H. A., and Montelione, G. T. (1997) NMR structural analysis of an analyog of an intermediate formed in the rate-determining step on one pathway in the oxidative folding of bovine pancreatic ribonuclease A: Automated analysis of ^{1}H, ^{13}C, and ^{15}N resonance assignments for wild-type and [C65S, C72S] mutant forms. *Biochemistry 36*, 6915–6929.
13. Laity, J. H., Lester, C. C., Shimotakahara, S., Zimmerman, D. E., Montelione, G. T., and Scheraga, H. A. (1997) Structural characterization of an analog of the major rate-determining disulfide-folding intermediate of bovine pancreatic ribonuclease A. *Biochemistry 36*, 12683–12699.
14. Gahl, R. F., Narayan, M., Xu, G., and Scheraga, H. A. (2008) Dissimilarity in the oxidative folding of onconase and ribonuclease A, two structural homologs. *Protein Eng., Des. Sel. 21* (4), 223–231.
15. Boix, E., Wu, Y., Vasandani, V. M., Saxena, S. K., Ardelt, W., Ladner, J., and Youle, R. J. (1996) Role of the N terminus in RNase A homologues: Differences in catalytic activity, ribonuclease inhibitor interaction and cytotoxicity. *J. Mol. Biol. 257*, 992–1007.
16. Laity, J. K., Shimotakahara, S., and Scheraga, H. A. (1993) Expression of wild-type and mutant bovine pancreatic ribonuclease A in *Escherichia coli*. *Proc. Natl. Acad. Sci. U.S.A. 90*, 615–619.
17. Ellman, G. L. (1959) Tissue sulfhydryl groups. *Arch. Biochem. Biophys. 82*, 70–77.
18. Bates, R. G. (1961) Amine buffers for pH control. *Ann. N.Y. Acad. Sci. 92*, 341.
19. Lide, D. R., Ed. (2008) Values of pH(SS) of Some Secondary Standards from Harned Cell I Measurements. In *CRC Handbook of Chemistry and Physics, 88th Edition (Internet Version)*, CRC Press/Taylor and Francis, Boca Raton, FL.
20. Flannery, B. P., Teukolsky, S. A., and Vetterling, W. T. (2007) *Numerical Recipes: The Art of Scientific Computing*, 3rd ed., Cambridge University Press, New York.
21. Straume, M., and Johnson, M. L. (1992) Monte Carlo method for determining complete confidence probability distributions of estimated model parameters. *Methods Enzymol. 210*, 117.
22. Box, G. E. P., and Muller, M. E. (1958) A note on the generation of random normal deviates. *Ann. Math. Stat. 29*, 610–611.
23. Thannhauser, T. W., Rothwarf, D. M., and Scheraga, H. A. (1997) Kinetic studies of the regeneration of recombinant hirudin variant 1 with oxidized and reduced dithiothreitol. *Biochemistry 36*, 2154.
24. Thannhauser, T., Konishi, Y., and Scheraga, H. A. (1987) Analysis for disulfide bonds in peptides and proteins. *Methods Enzymol. 143*, 115–119.
25. Jocelyn, P. C. (1987) Chemical reduction of disulfides. *Methods Enzymol. 143*, 246–256.
26. Rothwarf, D. M., and Scheraga, H. A. (1993) Regeneration of bovine pancreatic ribonuclease A. 3. Dependence on the nature of the redox agent. *Biochemistry 32*, 2690–2697.
27. Harrington, W. F., and Schellman, J. A. (1956) Evidence for the instability of hydrogen-bonded peptide structures in water, based on studies of ribonuclease and oxidized ribonuclease. *C. R. Trav. Lab. Carlsberg, Ser. Chim. 30*, 21–43.
28. Hermans, J., Jr., and Scheraga, H. A. (1961) Structural studies of ribonuclease. V. Reversible change of configuration. *J. Am. Chem. Soc. 83*, 3283–3292.
29. Matheson, R. R., Jr., and Scheraga, H. A. (1978) A method for predicting nucleation sites for protein folding based on hydrophobic contacts. *Macromolecules 11*, 819–829.
30. Kauzmann, W. (1959) Some factors in the interpretation of protein denaturation. *Adv. Protein Chem. 14*, 1–63.
31. Nemethy, G., and Scheraga, H. A. (1962) The structure of water and hydrophobic bonding in proteins. II. A model for the thermodynamic properties of aqueous solutions of hydrocarbons. *J. Chem. Phys. 36*, 3401–3417.
32. Nemethy, G., and Scheraga, H. A. (1962) The structure of water and hydrophobic bonding in proteins. III. The thermodynamic properties of hydrophobic bonds in proteins. *J. Phys. Chem. 66*, 1773–1789.
33. Narayan, M., Xu, G., Ripoll, D. R., Zhai, H., Breuker, K., Wanjalla, C., Leung, H. J., Navon, A., Welker, E., McLafferty, F. W., and Scheraga, H. A. (2004) Dissimilarity in the reductive unfolding pathways of two ribonuclease homologues. *J. Mol. Biol. 338*, 794–809.
34. Lin, S. H., Konishi, Y., Denton, M. E., and Scheraga, H. A. (1984) Influence of an extrinsic cross-link on the folding pathway of ribonuclease A. Conformational and thermodynamic analysis of cross-linked (lysine7-lysine41)-ribonuclease A. *Biochemistry 23*, 5504–5512.

BI802327J